MATERIALS CHEMISTRY
FRONTIERS

RESEARCH ARTICLE

View Article Online
View Journal | View Issue

Cite this: *Mater. Chem. Front.*, 2018, **2**, 514

Tris(2-hydroxyphenyl)triazasumanene: bowl-shaped excited-state intramolecular proton transfer (ESIPT) fluorophore coupled with aggregation-induced enhanced emission (AIEE)†

Patcharin Kaewmati,[a] Yumi Yakiyama,[a] Hiroyoshi Ohtsu,[b] Masaki Kawano,[b] Setsiri Haesuwannakij,[c] Shuhei Higashibayashi[d] and Hidehiro Sakurai*[a]

Received 15th November 2017,
Accepted 15th January 2018

DOI: 10.1039/c7qm00530j

rsc.li/frontiers-materials

Tris(2-hydroxyphenyl)triazasumanene ((*A*)-(+)-**1**), a bowl-shaped molecule, which possesses 2-(2′-hydroxyphenyl)pyridine moieties, was successfully synthesised. (*A*)-(+)-**1** showed a single peak emission in CH_2Cl_2, which overlapped with the emission of the triazasumanene skeleton and diminished at a high concentration, corresponding to the formation of the excited enol form. In contrast, single crystals of (*A*)-(+)-**1** exhibited a dual emission with a large Stokes shift, indicating the presence of the excited keto form by the excited state intramolecular proton transfer (ESIPT) process. In the solution of (*A*)-(+)-**1** containing a mixture of a large amount of a poor solvent (hexane or MeOH) and a small amount of CH_2Cl_2, colloidal aggregates emerged with the continuous increment of emission intensity by further addition of the poor solvent, demonstrating aggregation-induced enhanced emission (AIEE). The analysis of the morphology and the structure of the aggregates using a scanning electron microscope (SEM) and powder X-ray diffraction (PXRD) revealed the well-ordered structure of the aggregates, which possessed a molecular packing pattern similar to that of an (*A*)-(+)-**1** single crystal.

Introduction

In the molecular design of organic emissive materials, which are receiving a lot of attention due to their wide application, one of the most important strategies is to introduce a key structure that exhibits a unique optical property. Excited state intramolecular proton transfer (ESIPT)[1] is a widely studied phenomenon in terms of its potential application for laser dyes,[2] ultraviolet (UV) photostabilizers,[3] photoswitches[4] and electroluminescent materials.[5] ESIPT occurs *via* an ultrafast reaction process to create a large Stokes shift (6000–12 000 cm^{-1}),[1a] which often shows dual emission. In general, dual emission consists of a shorter wavelength one derived from the excited state enol form (E*) and a longer wavelength one due to the excited state keto form (K*). ESIPT is also well known to be very sensitive to the surrounding environment, such as the solvent system and acidic conditions. As a minimum requirement to realise this unique property of ESIPT, a preformed intramolecular hydrogen bond (H-bond) between the proton donor (–OH, $–NH_2$) and the proton acceptor (–C═O, –N═) groups must be in close proximity to each other in a molecule.

Triazasumanene (TAS) is a C_3-symmetric chiral azabucky-bowl, a nitrogen analogue of sumanene,[6] and it possesses three peripheral pyridine skeletons (Fig. 1).[7] Previously, we reported on the enantioselective synthesis of trisubstituted C_3-symmetric TAS derivatives with MeS (**2**), $MeSO_2$ and various aryl groups.[7] These were found to have unique properties, such as a deeper bowl depth (1.30 Å for tri-$MeSO_2$; 1.27–1.28 Å for tri-(4-CF_3Ph) derivatives) than that of pristine sumanene (1.11 Å), and high

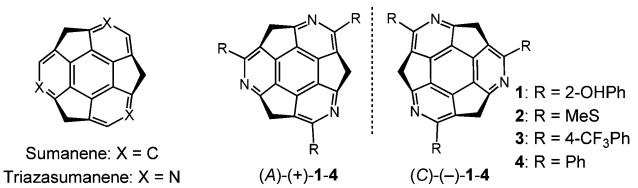

Fig. 1 Molecular structures of sumanene and triazasumanenes.

[a] *Division of Applied Chemistry, Graduate School of Engineering, Osaka University, 2-1 Yamadaoka, Suita, Osaka 565-0871, Japan. E-mail: hsakurai@chem.eng.osaka-u.ac.jp*
[b] *Department of Chemistry, Graduate School of Science and Engineering, Tokyo Institute of Technology, 2-12-1 Ookayama, Meguro-ku, Tokyo 152-8551, Japan*
[c] *School of Molecular Science & Engineering, Vidyasirimedhi Instituteof Science and Technology (VISTEC), 555 Moo 1 Payupnai, Wangchan, Rayong 21210, Thailand*
[d] *Faculty of Pharmacy, Keio University, 1-5-30 Shibakoen, Minato-ku, Tokyo 105-8512, Japan*

† Electronic supplementary information (ESI) available. CCDC 1552563. For ESI and crystallographic data in CIF or other electronic format see DOI: 10.1039/c7qm00530j

bowl inversion energy (*ca.* 40 kcal mol^{-1} for tri-MeS derivative), which enables the successful separation of two enantiomers defined by the inherent bowl chirality of TAS (*cf.* 20.3 kcal mol^{-1} for pristine sumanene).[6c] These features are attributable to nitrogen doping on the sumanene skeleton. These findings encouraged us to further study the functionalisation of the TAS skeleton with the expectation of identifying additional aspects. In the present study, we synthesised three 2-hydroxyphenyl group-introduced TAS as a single enantiomer (*A*)-(+)-tris(2-hydroxyphenyl)triazasumanene ((*A*)-(+)-**1**). Spectroscopic analyses revealed that single crystals of (*A*)-(+)-**1** can exhibit the dual emission caused by ESIPT. This finding was also supported by the single crystal X-ray analysis, which showed the formation of strong OH···N type hydrogen bonds. Further investigation using solvent- and concentration-dependent emission spectra led us to find that (*A*)-(+)-**1** can also exhibit aggregation-induced enhanced emission (AIEE),[8] which is one of the effective methods used to obtain highly emissive solid materials. An AIEE-active system coupled with ESIPT[9] is still rare, and this paper presents the first example of the curved-π molecule-based AIEE-active system coupled with ESIPT.[10]

Results and discussions

Synthesis and crystal structure of (*A*)-(+)-1

The synthesis of (*A*)-(+)-**1** was performed using the previously reported cross-coupling reaction of (*A*)-(+)-tris(methylthio)-triazasumanene ((*A*)-(+)-**2**) with 2-hydroxyphenylboronic acid.[7] A tetrahydrofuran (THF) solution of (*A*)-(+)-**2**, $Pd_2(dba)_3$ (20 mol%), 2-hydroxyphenylboronic acid (500 mol%), tri(2-furyl)phosphine (TFP, 100 mol%) and Cu(I)thiophene carboxylate (CuTC, 500 mol%) were heated at 50 °C to afford (*A*)-(+)-**1** in 80% yield as a yellow solid (Scheme 1). In ^{1}H NMR (in $CDCl_3$), the peak assignable to phenol hydroxyl proton appeared with significant downfield shift at 13.4 ppm, indicating the formation of stable intramolecular hydrogen bond (ESI†).

Single crystal X-ray analysis revealed the unique packing structure of (*A*)-(+)-**1** in its crystalline state. In the structure, there is only one crystallographically independent (*A*)-(+)-**1** because the three sets of the dihedral angles around the three peripheral pyridine rings on the TAS skeleton and the three phenol rings connecting to them were slightly different (Fig. 2a). On the (*A*)-(+)-**1** skeleton, three intramolecular OH···N type hydrogen bonds were observed between the phenol hydroxy group and the N atom on the peripheral pyridine skeleton. Their O···N lengths (2.554(2)–2.588(2) Å) were shorter than the general

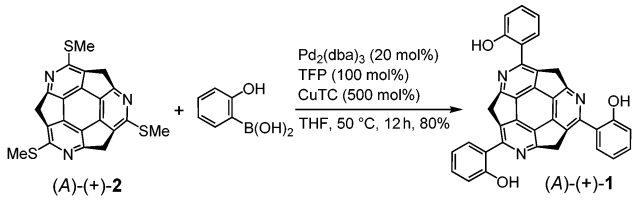

Scheme 1 Synthesis of (*A*)-(+)-**1**.

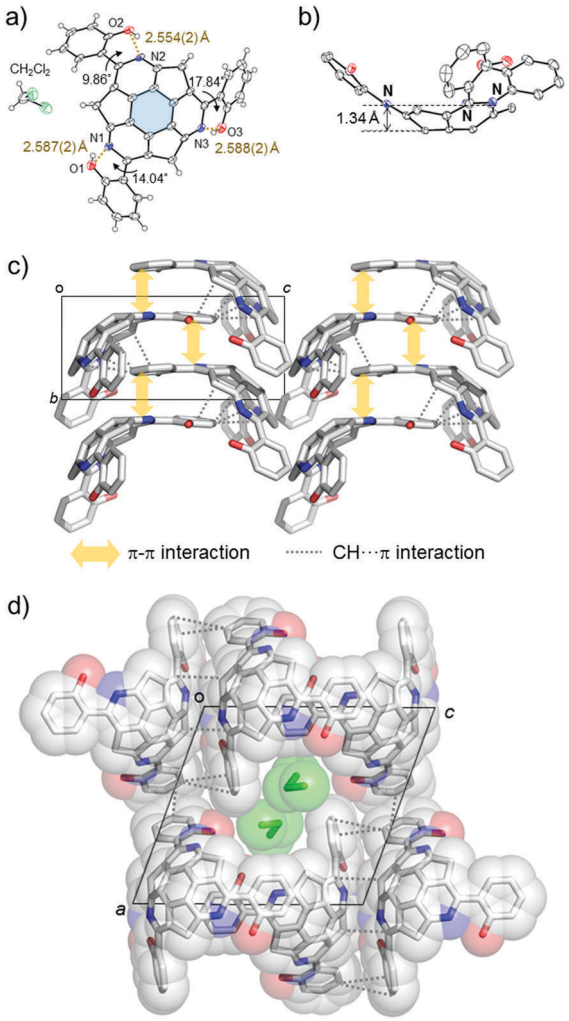

Fig. 2 Crystal structure of (*A*)-(+)-**1**. (a) ORTEP model of (*A*)-(+)-**1**. The brown dotted lines show the intramolecular hydrogen bonds. (b) The deepest position of the bowl depth. In (a and b), the ellipsoids are shown in 50% probability. (c) Stacking structure viewed from the *b* axis with intermolecular π–π (yellow solid arrow) and CH···π (grey dotted line) interactions. (d) One-dimensional channel structure with intercolumnar CH···π interactions. Green molecules correspond to the encapsulated CH_2Cl_2. The colour codes in each of the images in this figure are: C, grey; N, blue; O, red; Cl, light green; however, (e) in (a), the hydrogen atoms are omitted for clarity.

OH···N type hydrogen bond distance (2.7–2.8 Å),[11] indicating the presence of a relatively strong attractive force within the three hydrogen bonds. The bowl depth, which can be defined by the distance between the centre of the hexagonal ring at the bottom of the TAS skeleton (blue part in Fig. 2a) and the plane, consisting of three N atoms (N1, N2 and N3), was 1.34 Å (Fig. 2b). This bowl depth was slightly deeper than the values that have been previously reported (*A*)-(+)-**2** (1.30 Å) and tris(*p*-trifluoromethylphenyl)triazasumanene (**3**) (1.27–1.28 Å).[7] Each (*A*)-(+)-**1** formed a CH···π and π–π interaction at the 2-(2′-hydroxyphenyl)pyridine moieties to give a slippery-stacked columnar structure along the *b* axis (Fig. 2c); hence, the TAS skeleton did not form the direct overlap, which is often found in sumanene derivatives due to the convex-concave-type stacking

structure.[6] These stacking columns resulted in additional CH···π interactions among the neighbouring columns to construct a one-dimensional channel structure along the *b* axis with the size of 5.8 Å × 3.5 Å, in which CH_2Cl_2 (0.25 Occ.) was encapsulated as the crystalline solvent (Fig. 2d).

Photophysical property of (*A*)-(+)-1

The ultraviolet-visible (UV-vis) spectra of (*A*)-(+)-**1** showed absorption maxima at 370 nm in the CH_2Cl_2 solution, which slightly red shifted to 382 nm in the single crystals of (*A*)-(+)-**1** (Fig. 3). The small UV peak shift may be simply attributed to the intermolecular interactions involved in the J-aggregation-like stacking structure of 2-(2′-hydroxyphenyl)pyridine moiety in the crystalline state (Fig. 2 and Fig. S1, ESI†). The emission spectrum of single crystals of (*A*)-(+)-**1** was significantly different from the spectrum measured in the CH_2Cl_2 solution. On excitation at 370 nm, the 4.0 × 10^{-5} M CH_2Cl_2 solution of (*A*)-(+)-**1** showed a single emission peak at 447 nm, and its intensity significantly reduced at a higher concentration due to the concentration quenching (Fig. 3 and Fig. S2, ESI†). In contrast, a large shift (294 nm) in the additional emission band (λ_{max} = 631 nm) was observed for the single crystals of (*A*)-(+)-**1**. Consequently, it was expected that (*A*)-(+)-**1** possesses the ESIPT-active 2-(2′-hydroxyphenyl)pyridine moiety,[12] which forms strong OH···N type hydrogen bonds in the crystal structure (Fig. 2a). This dual emission can be explained by the ESIPT effect at the 2-(2′-hydroxyphenyl)pyridine moiety of (*A*)-(+)-**1**. Therefore, the lower energy emission at 631 nm can be assigned to the K* form. The structured higher energy emission at around 410–500 nm was well overlapped with the single emission observed in the CH_2Cl_2 solution. Therefore, it might be easy to assign this to the E* form of emission. However, a similar emission was also observed in non-ESIPT-active triphenyltriazasumanene (**4**) and **3** together with another broad band around 540–590 nm (Fig. S3, ESI†).[7] All these peaks were attributed to the TAS-skeleton, and therefore, the structured emission should be assigned to the mixture of the TAS skeleton-based structures rather than the E* form.[13] In the CH_2Cl_2 solution, the contribution of the E* form might be larger than it is in the solid state because the fast rotation of the 2-hydroxyphenyl ring in CH_2Cl_2 restricts the ESIPT process *via* the formation of the OH···N type hydrogen bond.[14] It would be interesting to know if these three OH···N hydrogen bonds contribute to the ESIPT process of (*A*)-(+)-**1** in a concerted process or in a stepwise process.[13,15]

The emission spectra of (*A*)-(+)-**1** were also recorded for different compositions of the CH_2Cl_2–hexane or MeOH mixtures (100 : 0 to 2 : 98; v/v) (Fig. 4 and Fig. S4, S5, ESI†). In the process of adding hexane, the emission intensity at around 430 nm, derived from both the TAS skeleton and the E* form, did not change much until the volumetric ratio was 80 : 20 (hexane : CH_2Cl_2). However, after the ratio was 90 : 10, the emission peak intensity at 430 nm suddenly increased and a new emission peak appeared at 634 nm, which was attributable to the K* form of (*A*)-(+)-**1**. Furthermore, at the same hexane : CH_2Cl_2 (90 : 10) ratio, we confirmed in the UV cell that the colloidal aggregates of (*A*)-(+)-**1a** dispersed homogeneously just after the appropriate amount of hexane was added to the CH_2Cl_2 stock solution. The amount of aggregates and the emission peak intensities at both 430 nm and 634 nm continuously increased as the ratio of hexane increased, indicating that (*A*)-(+)-**1** is AIEE active. The relative ratio of both emission intensities was completely different from those of the crystalline sample (Fig. 3). This can be explained by the fact that the emission at around 430 nm includes the emission from the aggregates as well as the emission from the saturated CH_2Cl_2 solution of (*A*)-(+)-**1**. In the case in which MeOH was added, we also confirmed that the AIEE

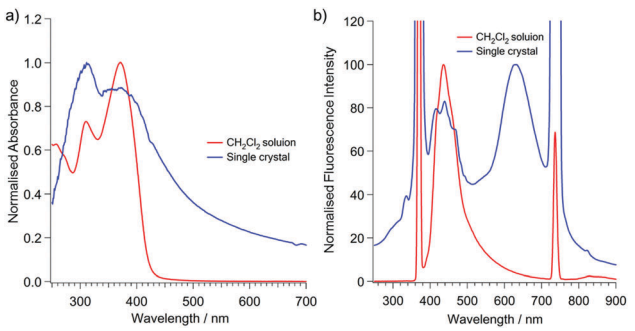

Fig. 3 Absorption (a) and emission (b) spectra of (*A*)-(+)-**1** at room temperature. Red: 4.0 × 10^{-5} M CH_2Cl_2 solution. Blue: single crystalline solid. λ_{ex} = 370 nm.

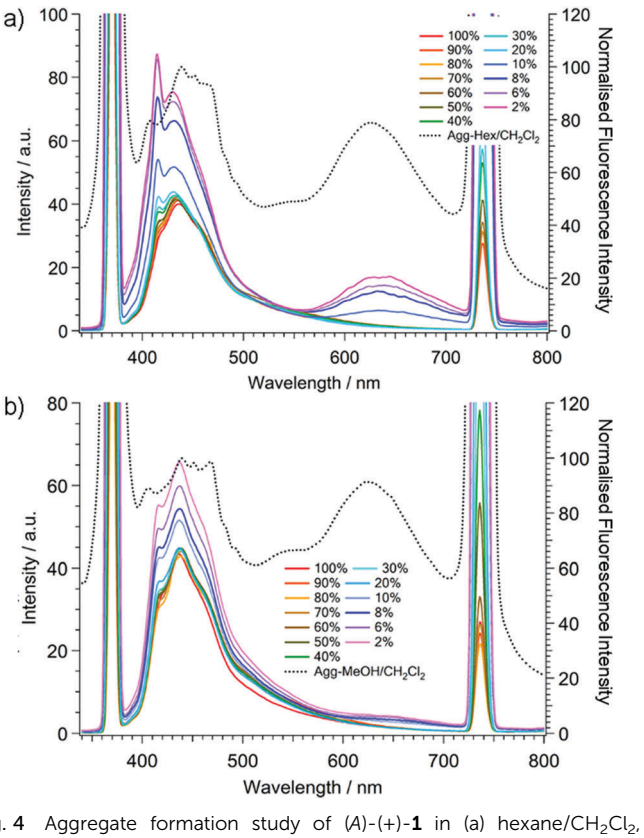

Fig. 4 Aggregate formation study of (*A*)-(+)-**1** in (a) hexane/CH_2Cl_2, (b) MeOH/CH_2Cl_2 systems. λ_{ex} = 370 nm. The annotation indicates the volumetric ratio of CH_2Cl_2 in each mixture. Dotted lines (*y* axis: right side) indicate the dried aggregates.

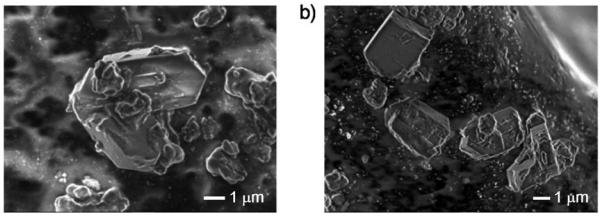

Fig. 5 SEM images of the dried-aggregates of (*A*)-(+)-**1**. (a) From the hexane/CH_2Cl_2 mixture. (b) From the MeOH/CH_2Cl_2 mixture.

phenomenon showed a continuous increment of the emission peaks at both 430 nm and 634 nm after the MeOH : CH_2Cl_2 volumetric ratio was 90 : 10. However, the emission from the K* form at 634 nm in the MeOH–CH_2Cl_2 mixture was much weaker than that of the hexane–CH_2Cl_2 mixture, and the magnitude of the intensity increment was very small even in the 98 : 2 MeOH–CH_2Cl_2 solution. This can simply be explained by the high polarity of MeOH, which disturbs the formation of the K* form by covering the hydrogen bonding moiety to exhibit the emission from the E* form dominantly after photo irradiation.[16]

Fig. 4 also shows the emission spectra of the aggregates after the removal of the solvent (dotted lines). Both dried aggregates exhibited dual emission spectra similar to that of the single crystals. In the emission spectra of both dried aggregates, the emission peak corresponding to the K* form was also observed at around 625 nm. Their relative intensity against the emission at around 430 nm was much stronger than in the case of non-dried aggregates. Meanwhile, the higher energy emission bands of the dried aggregates at around 430 nm were broader than those of the non-dried aggregates, also indicating that the intermolecular interaction between (*A*)-(+)-**1** and the solvents has a strong impact on their emission properties. In addition, these results indicate that both of the dried aggregates, wherever they formed, constructed specific molecular arrangements, inducing AIEE.

To obtain further insights about the structure of the aggregated products of (*A*)-(+)-**1**, scanning electron microscope (SEM) measurements and powder X-ray diffraction (PXRD) studies were performed (Fig. 5 and Fig. S6, ESI†). The SEM images of the aggregates prepared from both the MeOH–CH_2Cl_2 and hexane–CH_2Cl_2 mixed solutions of (*A*)-(+)-**1** revealed the formation of microcrystals. The PXRD analysis of all the dried aggregates, which showed diffraction patterns indicating the presence of the crystalline species, also supported the SEM observations. Their diffraction patterns were similar to that of the simulated pattern obtained from the single crystal data, indicating that all the aggregates possess a molecular packing structure similar to that of the single crystal of (*A*)-(+)-**1**, which realised the solid-state emission.

Conclusion

As described in this paper, we successfully synthesised tris(2-hydroxyphenyl)triazasumanene (*A*)-(+)-**1** as a new non-planar ESIPT fluorophore model of a curved-π molecule-based AIEE-active system coupled with ESIPT. The single crystal analysis revealed the J-aggregation-like packing pattern of 2-hydroxyphenyl moieties on (*A*)-(+)-**1** to prevent the formation of a strong π–π stacking column in the TAS skeleton. This single crystalline (*A*)-(+)-**1** showed dual emission due to the ESIPT process. This solvent- and concentration-dependent emission study exhibited that (*A*)-(+)-**1** achieved AIEE at the large volumetric ratio of the poor solvent. The SEM and PXRD measurements of the aggregates of (*A*)-(+)-**1** revealed the formation of crystalline materials with a molecular arrangement similar to that of single crystalline state, which exhibits a solid-state emission.

Experimental section

General information

Chemical reagents and solvents were commercially purchased and purified according to the standard methods, if necessary. Air- and moisture-sensitive reactions were carried out using commercially available anhydrous solvents under an inert atmosphere of nitrogen. ^{1}H and ^{13}C NMR spectra were recorded on 400 MHz JEOL JNM-ECS400 NMR spectrometer (^{1}H: 400 MHz and ^{13}C: 100 MHz). Chemical shifts (δ) are expressed relative to the resonances of the residual non-deuterated solvent for ^{1}H ($CDCl_3$: ^{1}H(δ) = 7.26 ppm) and for ^{13}C ($CDCl_3$: ^{13}C(δ) = 77.0 ppm). Solution state UV-vis absorption and emission spectra were recorded on a JASCO V-670 spectrophotometer and a FP-6500 spectrofluorometer using 1 cm^{-1} path-length quartz cells, respectively. Solid state UV-vis absorption spectra of the single crystals of (*A*)-(+)-**1** dispersed in $BaSO_4$ powder was recorded on a JASCO V-670 spectrophotometer with an integrating sphere. High-resolution fast atom bombardment (FAB) mass spectra were measured on a JEOL JMS-700 spectrometer. Melting points were determined on a Stanford Research Systems Optimelt MPA100 and were uncorrected. The SEM images were measured on a JEOL JSM-7610F field emission scanning electron microscope. Powder diffraction X-ray analysis (PXRD) data were recorded by using Rigaku RINT-2000 using graphite-monochromitized Cu-Kα radiation (λ = 1.54187 Å) at room temperature. The preparative TLC (PTLC) purification was conducted using Wakogel B-5F PTLC plates. The quantum chemical calculation was performed at the CAM-B3LYP/6-31G+(d,p) level[17] with Gaussian 09 program.[18]

Synthesis of tris(2-hydroxyphenyl)triazasumaene (*A*)-(+)-1

A solution of $Pd_2(dba)_3$ (2.3 mg, 0.0025 mmol) and tris(2-furyl)-phosphine (2.8 mg, 0.012 mmol) in THF (200 μL) was added to a mixture of tris(methylthio)triazasumanene ((*A*)-(+)-**1**)[4] (5.0 mg, 0.012 mmol), 2-hydroxyphenylboronic acid (8.5 mg, 0.062 mmol) and CuTC (11.8 mg, 0.0617 mmol) in THF (3 mL) under N_2 atmosphere. The mixture was stirred at 50 °C under N_2 condition for 12 h, then cooled to room temperature and quenched with 28% NH_3 aqueous solution in brine (1 : 1 (v/v), 10 mL). The mixture was then stirred for 10 min and extracted with CH_2Cl_2 for 3 times. The combined organic layer was dried over anhydrous Na_2SO_4, filtered and concentrated under reduced pressure.

The residue was purified by silica gel preparative TLC using CH_2Cl_2 as eluent to afford (*A*)-(+)-**1** (5.3 mg, 80% yield) as a yellow solid. Single crystals for X-ray structure analysis were obtained by slow evaporation method from CH_2Cl_2.

R_f = 0.60 (CH_2Cl_2); m.p.: 139 °C (dec.); $[\alpha]_D^{20}$ = +278 (*c* = 0.12, CH_2Cl_2); ^{1}H NMR (400 MHz, $CDCl_3$) δ (ppm) 13.42 (s, 3H), 7.80 (dd, *J* = 7.6, 1.6 Hz, 3H), 7.33 (ddd, *J* = 16.8, 8.4, 1.6 Hz, 3H), 7.03 (ddd, 16.0, 8.4, 1.6, 3H), 6.99 (dd, *J* = 7.6, 1.6 Hz, 3H), 5.32 (d, *J* = 19.2 Hz, 3H), 3.59 (d, *J* = 20.0 Hz, 3H); ^{13}C NMR (100 MHz, $CDCl_3$) δ (ppm) 172.3, 160.7, 160.0, 158.2, 140.4, 135.6, 132.2, 130.1, 119.6, 119.1, 118.5, 45.5; IR (KBr): ν (cm^{-1}) 2956, 1616, 1577, 1548, 1463, 1396, 1363, 1295, 1249, HRMS (FAB) *m*/*z* calcd for $C_{36}H_{27}N_3$ [M + H$^+$]: 544.1661. Found: 544.1679.

Crystal data for (*A*)-(+)-1

The diffraction data for (*A*)-(+)-**1** was recorded on a ADSC Q210 CCD area detector with a synchrotron radiation (λ = 0.70000 Å) at 2D beamline in Pohang Accelerator Laboratory (PAL) at 100 K. The diffraction images were processed by using HKL3000. The structures were solved by direct methods (SHELXS) and refined by full-matrix least squares calculations on F^2 (SHELXL) using the Olex2 program package.

$C_{36}H_{21}N_3O_3(CH_2Cl_2)_{0.24}$, M_w = 564.36, crystal dimensions 0.04 × 0.03 × 0.02 mm^3, monoclinic, space group = $P2_1$, *a* = 14.1631(1) Å, *b* = 6.8184(1) Å, *c* = 15.4813(1) Å, β = 109.465(3)°, *V* = 1409.58(3) Å^3, *T* = −173 °C, *Z* = 2, ρ_{calcd} = 1.330 g cm^{-3}, μ = 0.91 cm^{-1}, 7287 unique reflections out of 8036 with $I > 2\sigma(I)$, 410 parameters, 2.657° < θ < 29.523°, R_1 = 0.0403, wR_2 = 0.1087, GOF = 1.063. Flack = −0.02(4). CCDC 1552563.†

Solid UV-vis and fluorescence spectra

Aggregate formation study. Stock CH_2Cl_2 solution of (*A*)-(+)-**1** (2 mM) was prepared. An aliquot (10 μL) of the stock solution was transferred to a 4.5 mL quartz cell. After adding an appropriate amount of CH_2Cl_2, poor solvent (hexane or MeOH) was added to furnish 40 μM CH_2Cl_2/hexane or CH_2Cl_2/MeOH mixtures where the poor solvent fractions was 0–98 vol%. The mixtures were stirred for 5 min at room temperature before recording fluorescence spectra.[19] The aggregates were collected by filtration using membrane filter, dried under reduced pressure and then used for emission spectra measurement. The resulting solids were also used for SEM and PXRD measurements.

Conflicts of interest

There are no conflicts to declare.

Acknowledgements

This study was supported by a Grant-in-Aid for Scientific Research on Innovative Area 'π Space Figuration' from MEXT (No. JP26102002), and JSPS KAKENHI (JP26288020). S. H. acknowledges ACT-C, JST (JPMJCR12YZ), for the support. Y. Y. acknowledges Ogasawara Foundation for the Promotion of Science & Engineering and Iketani Science and Technology Foundation for the support. We thank Prof. Norimitu Tohnai for the help of PXRD measurement. The X-ray diffraction study of (*A*)-(+)-**1** with synchrotron radiation was performed at the Pohang Accelerator Laboratory (Beamline 2D) supported by POSTECH.

Notes and references

1 Recent review of ESIPT, see; (*a*) J. E. Kwon and S. Y. Park, *Adv. Mater.*, 2011, **23**, 3615–3642; (*b*) V. S. Padalkar and S. Seki, *Chem. Soc. Rev.*, 2016, **45**, 169–202.
2 K. Sakai, T. Tsuzuki, Y. Itoh, M. Ichikawa and Y. Taniguchi, *Appl. Phys. Lett.*, 2005, **86**, 081103.
3 M. J. Paterson, M. A. Robb and L. Blancafort, *J. Phys. Chem. A*, 2005, **109**, 7527–7537.
4 A. L. Sobolewski, *Phys. Chem. Chem. Phys.*, 2008, **10**, 1243–1247.
5 S. Park, J. E. Kwon, S. H. Kim, J. Seo, K. Chung, S.-Y. Park, D.-J. Jang, B. M. Medina, J. Gierschner and S. Y. Park, *J. Am. Chem. Soc.*, 2009, **131**, 14043–14049.
6 (*a*) H. Sakurai, T. Daiko and T. Hirao, *Science*, 2003, **301**, 1878; (*b*) H. Sakurai, T. Daiko, H. Sakane, T. Amaya and T. Hirao, *J. Am. Chem. Soc.*, 2005, **127**, 11580–11581; (*c*) T. Amaya, H. Sakane, T. Muneishi and T. Hirao, *Chem. Commun.*, 2008, 765–767; (*d*) T. Amaya, S. Seki, T. Moriuchi, K. Nakamoto, T. Nakata, H. Sakane, A. Saeki, S. Tagawa and T. Hirao, *J. Am. Chem. Soc.*, 2009, **131**, 408–409; (*e*) S. Higashibayashi, R. B. N. Baig, Y. Morita and H. Sakurai, *Chem. Lett.*, 2012, **41**, 84–86; (*f*) S. Mebs, M. Weber, P. Luger, B. M. Schmidt, H. Sakurai, S. Higashibayashi, S. Onogi and D. Lentz, *Org. Biomol. Chem.*, 2012, **10**, 2218–2222.
7 (*a*) Q. Tan, S. Higashibayashi, S. Karanjit and H. Sakurai, *Nat. Commun.*, 2012, **3**, 891; (*b*) P. Kaewmati, Q. Tan, S. Higashibayashi, Y. Yakiyama and H. Sakurai, *Chem. Lett.*, 2016, **46**, 146–148.
8 J. Mei, N. L. C. Leung, R. T. K. Kwok, J. W. Y. Lam and B. Z. Tang, *Chem. Rev.*, 2015, **115**, 11718–11940.
9 (*a*) Y. Qian, S. Li, G. Zhang, Q. Wang, S. Wang, H. Xu, C. Li, Y. Li and G. Yang, *J. Phys. Chem. B*, 2007, **111**, 5861–5868; (*b*) R. Hu, S. Li, J. Chen, S. Wang, Y. Li and G. Yang, *Phys. Chem. Chem. Phys.*, 2011, **13**, 2044–2051; (*c*) A. Kindu, P. S. Harihasan, K. Prabakaran, D. Moon and S. P. Anthony, *Cryst. Growth Des.*, 2016, **116**, 3400–3408.
10 Recently, aggregation induced emission (AIE) active curved-π molecule has been reported. See; S. H. Mahadevegowda and M. C. Stuparu, *Eur. J. Org. Chem.*, 2017, 570–576.
11 *Crystal Engineering*, ed. G. R. Desiraju, J. J. Vittal and A. Ramanan, World Scientific, 2011.
12 (*a*) D. LeGourriérec, V. Kharlanov, R. G. Brown and W. Rettig, *J. Photochem. Photobiol., A*, 1998, **117**, 209–216; (*b*) N. Basaric and P. Wan, *Photochem. Photobiol. Sci.*, 2006, **5**, 656–664.
13 A time-dependent density functional theory (TD-DFT) calculation-based detailed discussion will be reported as an independent paper.
14 R. Hu, S. Li, Y. Zeng, J. Chen, S. Wang, Y. Li and G. Yang, *Phys. Chem. Chem. Phys.*, 2011, **13**, 2044–2051.

15 R. Pradhan, A. K. Harshan, G. S. K. Chandrika, A. Srinivasan and U. Lourderaj, *J. Phys. Chem. A*, 2016, **120**, 9894–9906.
16 F. Rodriguez-Prieto, J. C. Penedo and M. Mosquera, *J. Chem. Soc., Faraday Trans.*, 1998, **94**, 2775–2782.
17 (*a*) D. Ghosh, S. Batuta, N. A. Begum and D. Mandal, *J. Lumin.*, 2017, **184**, 64–73; (*b*) Y. Peng, Y. Ye, X. Xiu and S. Sun, *J. Phys. Chem. A*, 2017, **121**, 5625–5634; (*c*) A. Szemik-Hojniak, Ł. Wiśniewski, I. Deperasińska, A. Makarewicz, L. Jerzykiewicz, A. Puszko, Y. Erez and D. Huppert, *Phys. Chem. Chem. Phys.*, 2012, **14**, 8147–8159; (*d*) M. Li, W. Ren, Z. He and Y. Zhu, *J. Cluster Sci.*, 2017, **28**, 2111–2122; (*e*) D. Jacquemin, A. Planchat, C. Adamo and B. Mennucci, *J. Chem. Theory Comput.*, 2012, **8**, 2359–2372.
18 M. J. Frisch, G. W. Trucks, H. B. Schlegel, G. E. Scuseria, M. A. Robb, J. R. Cheeseman, G. Scalmani, V. Barone, G. A. Petersson, H. Nakatsuji, X. Li, M. Caricato, A. Marenich, J. Bloino, B. G. Janesko, R. Gomperts, B. Mennucci, H. P. Hratchian, J. V. Ortiz, A. F. Izmaylov, J. L. Sonnenberg, D. Williams-Young, F. Ding, F. Lipparini, F. Egidi, J. Goings, B. Peng, A. Petrone, T. Henderson, D. Ranasinghe, V. G. Zakrzewski, J. Gao, N. Rega, G. Zheng, W. Liang, M. Hada, M. Ehara, K. Toyota, R. Fukuda, J. Hasegawa, M. Ishida, T. Nakajima, Y. Honda, O. Kitao, H. Nakai, T. Vreven, K. Throssell, J. A. Montgomery, Jr., J. E. Peralta, F. Ogliaro, M. Bearpark, J. J. Heyd, E. Brothers, K. N. Kudin, V. N. Staroverov, T. Keith, R. Kobayashi, J. Normand, K. Raghavachari, A. Rendell, J. C. Burant, S. S. Iyengar, J. Tomasi, M. Cossi, J. M. Millam, M. Klene, C. Adamo, R. Cammi, J. W. Ochterski, R. L. Martin, K. Morokuma, O. Farkas, J. B. Foresman and D. J. Fox, *Gaussian 09*, Gaussian, Inc., Wallingford CT, 2016.
19 The fluorescence intensity continued to increase even more than 6 h after the sample preparation (Fig. S7, ESI†). For data collection, we stirred the mixtures for 5 min and quickly applied to measure emission spectra.